Journal of Medicinal Chemistry

Article

pubs.acs.org/jmc

Aggregation Induced Emission Mediated Controlled Release by Using a Built-In Functionalized Nanocluster with Theranostic Features

Zhan Zhou,[‡] Cheng Cheng Zhang,[∥] Yuhui Zheng,[‡] and Qianming Wang*[,†,‡,§]

[†]Key Laboratory of Theoretical Chemistry of Environment, Ministry of Education, School of Chemistry & Environment, South China Normal University, Guangzhou 510006, China

[‡]School of Chemistry & Environment, South China Normal University, Guangzhou 510006, China

[§]Guangzhou Key Laboratory of Materials for Energy Conversion and Storage, Guangzhou 510006, P. R. China

[∥]Departments of Physiology and Developmental Biology, University of Texas, Southwestern Medical Center, Dallas, Texas 75390-9133, United States

Supporting Information

ABSTRACT: We report biological evaluation of a novel nanoparticle delivery system based on 1,1,2-triphenyl-2-(*p*-hydroxyphenyl)-ethene (TPE-OH, compound **1**), which has tunable aggregation-induced emission (AIE) characteristics. Compound **1** exhibited no emission in DMSO. In aqueous media, compound **1** aggregated, and luminescence was observed. The novel membrane−cytoplasm−nucleus sequential delivery strategy could induce apoptosis in four different kinds of cancer cells (including three adherent cell lines and one suspension cell line). The nanoparticles remained in the cytoplasm with intense blue emissions, whereas doxorubicin was observed in the nucleus with striking red luminescence. The nanoassembly was internalized in cells through an energy-dependent process. Three sorts of chemical inhibitors were used to clarify the endocytosis mechanism based on the AIE type prodrug. Furthermore, we have developed the first AIE theranostic system where drug targeting and release have been applied in an animal model.

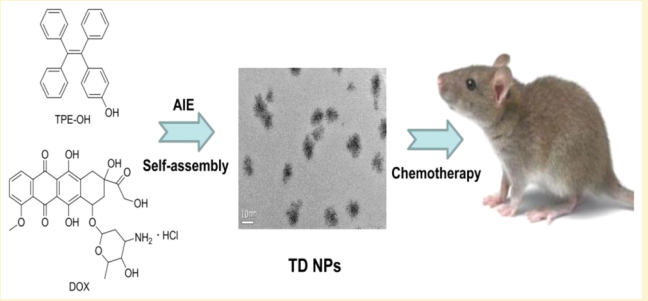

INTRODUCTION

The majority of human cancers are solid tumors. Therapeutic efficacy relies on delivery of the anticancer drugs to tumor cells. Chemotherapeutic agents must be transported across vascular walls into blood and, finally, must enter target cancer cells.[1,2] Often penetration, accumulation, and retention of therapeutic regents in tumor cells are very limited.[3,4] In order to circumvent the obstacles, novel nanoplatforms with high loading capacities and delivery capabilities have been reported.[5−10] In this way, the small-molecule drugs have been loaded onto the nanoscale delivery systems and are ready for releasing at particular tumor sites within physiological environments based on stimulus-responsive features, such as temperature, magnetic or electric field, and enzymatic and ultrasound triggers.[11−15]

Among the above external activations, several studies have offered deeper insights into drug delivery in a controllable manner derived from fluorescent signals.[16,17] However, overlap in emissions between the luminescent dyes and the drug molecules and quenching due to the biological environment prohibits the real-time monitoring of the therapeutic agents when this strategy is used. In addition, the low molecular weight molecules will automatically accumulate onto the surfaces of biological structures and the typical concentration quenching phenomenon would be a main disadvantage for the design of biosensors used in on-site detection. To circumvent these issues, Tang and his team members invented compounds that emit light upon aggregate formation,[18−20] and numerous aggregation-induced emission (AIE) species have now been synthesized.[21,22] Therefore, systems capable of tumor targeting based on AIE species have been prepared.[23,24] Hence, as described in Figure 1, we developed a self-emissive nanoscale prodrug in terms of the novel tetraphenylethylene bearing hydroxyl group (abbreviated as TPE-OH, compound **1**). The anticancer agent doxorubicin (DOX) was formulated with **1** in stable nanoassemblies (abbreviated as TD NPs).

This new theranostic method has provided an appealing chance by which the therapeutic process will be connected with the self-indicating diagnostic imaging. The potential strategy includes the detection and treatment of the disease at the same time. It is highly expected to fabricate the apoptosis related biochemical theranostic system that could finely monitor the specific response in the situation, but the biological behavior of AIE and DOX nanoparticles, especially concerning their cellular

Received: October 16, 2015

DOI: 10.1021/acs.jmedchem.5b01622
J. Med. Chem. XXXX, XXX, XXX−XXX

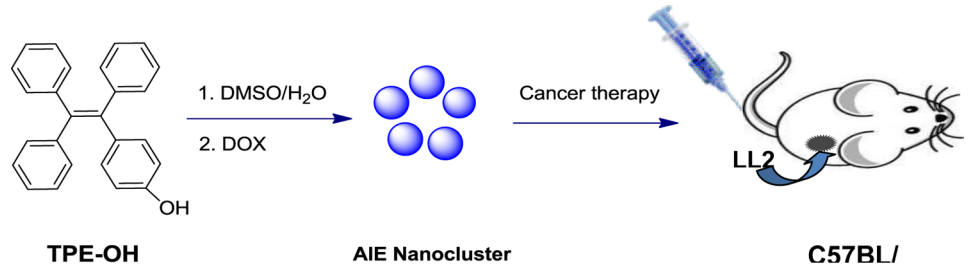

Figure 1. Representation of functionalized TD NPs used for LL2 tumor therapy in a mice model.

uptake mechanism, is not well understood. Exploring the principles of how nanodomains could pass through cell membranes would clarify the complicated pathways and decrease the risk of toxic effects. Here we used three different chemical inhibitors (chlorpromazine, cytochalasin D, and methyl-β-cyclodextran) to investigate the particular forms of endocytosis, and the basic results contribute to identify cellular entry modes. The elucidation of the exact transport channels based on AIE including nano pro-drug has never been reported.

The majority of current nanoscaled drug delivery systems have been concentrated on the cellular levels and the relations between independent tumor cells, and chemotherapeutic agents were emphasized. But the performance of bioassays and therapy in an animal model seems to be a real challenge, since complex structures, such as solid tumors, are not a group of individual cells and they reside in complex microenvironments. The vascular density and low diffusion rate will be the main drug transport barriers when the nanoparticles penetrate through the solid tissue to reach the target cancer cells. With the aim of studying the effects of drug release in tumor-affected tissues, the tumor-bearing mice were treated with the promising fluorescent nanoassembly to assess cancer targeting and organ distribution. To the best of our knowledge, this is the first example of drug targeting and release through an AIE based nanoplatform in vivo.

RESULTS AND DISCUSSION

Formulation and photophysical characterization of an AIE based drug delivery system. The structure of compound **1** is shown in Figure S1; the compound was synthesized in one step, as previously described.[25] Benzophenone was cross-coupled with 4-hydroxyl-phenylbenzophenone in dried THF under nitrogen atmosphere using Zn powder as the catalyst to give the target 1,1,2-triphenyl-2-(*p*-hydroxyphenyl)-ethene (compound **1**). Before performing the cell imaging and in vivo therapy, we tried to study whether the non-benigh solvent (here is water) was able to induce the molecular aggregations in TPE-OH (denoted as TPE-OH NPs). The changes in the emission features were expressed by using the steady-state fluorescence spectra. In DMSO, compound **1** exhibited almost no emission (Figure 2), likely due to the free rotation of the aromatic rings.[26] As the percentage of water was increased to 99%, a 50-fold enhancement in the blue emission band located at 465 nm was observed (Figure 2). The turn-on fluorescent signal was completely consistent with the observation (from invisible to bright blue) of the solutions under UV light irradiation (inset of Figure 2). To determine whether **1** was able to encapsulate an anticancer drug, we used doxorubicin (DOX) as a model. This positively charged molecule could be encapsulated into the nanocarriers due to electrostatic attractions and $\pi-\pi$ stacking interactions.[27] Under

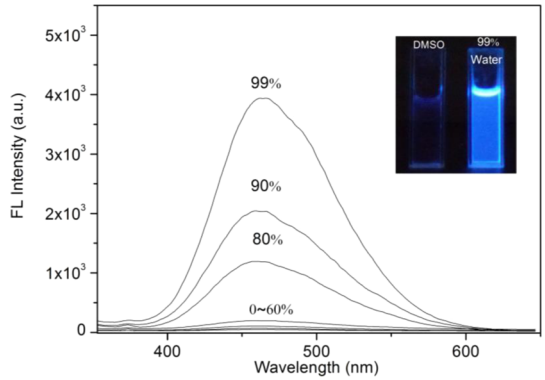

Figure 2. Photoluminescence spectra of TPE-OH (50 μM) in DMSO/water mixtures with different concentrations of water.

excitation at 330 nm, an immediate change was observed, and the emission band located at 465 nm has decreased, since the drug loading ratio was set as 10% (from blue line to red line in Figure S2). It is estimated that the adjacent species between TPE-OH NPs and DOX represented the existence of the Forster resonance energy transfer (FRET) channel. But the emission quenching from TPE-OH nanoparticles was also accompanied by the reduction (from green line to purple line in Figure S2) in the optical features from DOX (Ex = 477 nm), indicating that TD NPs could largely increase local DOX concentration and caused the aggregation induced quenching of light emissions (peak at 595 nm). To get insight into the FRET process, the emission of TPE-OH nanoparticles and the absorption of DOX were evaluated (Figure S3). The good spectral overlap between the donor and acceptor again confirmed the effectiveness of FRET.

An efficient method that provides the concurrent release of the optical signal changes and therapeutic agent would be highly preferable to curing cancers.[28,29] It has been discussed before that the improved drug release rate under lower pH values would be desirable in tumor therapy.[29,30] Here the capability of tunable drug delivery of AIE based carriers has been demonstrated by the activation of the prodrug via the pH-dependent process. As presented in Figure S4, no discernible changes in the fluorescence intensities were observed between neutral and acidic conditions, suggesting that TPE-OH nanoassembly was maintained almost stable during the release stage. In the case of DOX (Figure S5), however, a substantial increase in the red emission has been detected in pH 5.0 solution. These attractive observations provide the possibility that the majority of drug molecules might reach the tumor targets due to the lower pH environment and the therapy efficiency would be enhanced.

Morphological studies, stabilities, and structural information. The microstructures of the aggregated species

DOI: 10.1021/acs.jmedchem.5b01622
J. Med. Chem. XXXX, XXX, XXX−XXX

were explored by TEM. The individual TPE-OH nanoparticles were irregularly shaped and had an average diameter of around 80 nm, proving that small fluorophore molecules would accumulate into nanoclusters in the presence of water (Figure S6). After the drug molecules were loaded (DOX molar ratio = 10%), well-resolved nanospheres with monodispersed features were achieved and have a uniform diameter of 10 nm (Figure 3). The dimensions of these tiny particles are in the desired size

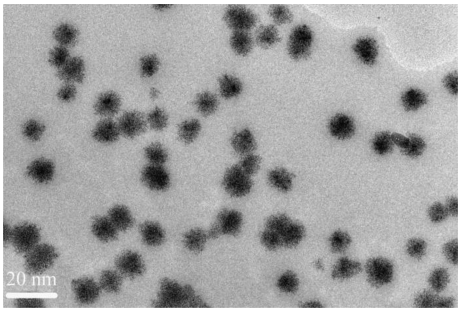

Figure 3. TEM image of nanoparticles of TPE-OH (50 μM) and 10% Dox formed in 99% of water.

range for tumor therapy and will be small enough for cell membrane penetration.[31−33] This dramatic change in morphology during the DOX incorporation process substantiated that the electrostatic forces contributed to the formation of the conjugate between donor and acceptor. This could be seen as an indication of effective delivery of DOX in TPE-OH nanoparticles. In order to explore the electrostatic forces between TPE-OH and DOX, we have investigated the zeta potentials of TPE-OH in the absence or presence of DOX. Results showed that the surface charge density decreased from −22.1 mV to −11.6 mV after DOX was incorporated, indicating that the electrostatic interaction existed between TPE-OH and DOX (Figure S7). With a higher concentration of DOX (molar ratio 15%), structures were nonuniform (Figure S8). The closer proximity between AIE aggregates and DOX (compared with independent TPE-OH nanoparticles) has been evaluated by the photoluminescence studies. It has been found that the blue emission was severely suppressed in the DOX concentration experiments and the peak wavelength slightly blue-shifted (Figure S9). According to the previous literature, the interactions with drug molecules may benefit for dispersing large aggregates in aqueous solution and facilitate the growth of small particles.[34] As for the stability of TD NPs, we measured the over quantum yields (Φ) through an integrating sphere method under room temperature. It has been found that the Φ value slightly changed even after 8 days (Figure S10). The results indicated that TD NPs could keep the assembled structures relatively stable. In addition, we also studied the thermostability of TD NPs at different temperatures. As given in Figure S11, the blue luminescence of TD NPs was maintained to be stable. At high temperature (60 °C), the reduction in peak emission intensity was around 10%. The FT-IR spectra of DOX, TPE-OH, and TD NPs were given in Figure S12. In the infrared curve of TPE-OH, the peaks at 3055 and 3015 cm^{-1} were ascribed to the unsaturated C−H stretching vibration. The intense band at 3525 cm^{-1} was caused by the O−H stretching vibration. In the curve of DOX, the peaks at 2981, 2932, and 2843 cm^{-1} were attributed to the saturated C−H stretching vibration. The peaks located at 3332 and 1730 cm^{-1} were assigned to the O−H and C═O stretching vibrations. In the case of TD NPs, the peaks of the C−H stretching vibration derived from DOX and the typical bands from TPE-OH were clearly identified and the results proved that TD NPs were formed. Moreover, the C═O absorption band of DOX shifted from 1730 to 1695 cm^{-1}, indicating that there might exist hydrogen bond interactions between DOX and TPE-OH. In order to figure out the local chemical composition of the assembled TD NPs, energy dispersive X-ray spectroscopy (EDX) was used (Figure S13). The EDX analysis provided a relative composition of TD NPs, and the corresponding elements C, N, O, and Cl were given in Table S1. The NMR spectrum of TD-NPs in DMSO-d_6 was provided in Figure S14.

Cell imaging features and behavior. Although the AIE effect will allow the uses of concentrated solutions with luminescence or their suspensions in aqueous environment for potential sensing purposes, the cases of successful live cell stain were very rare due to their poor solubilities.[35,36] To evaluate the feasibility of TPE-OH NPs as a novel optical marker for living cells imaging, mouse lewis lung carcinoma cells (LL2 cell) were incubated with AIE molecules (TPE-OH NPs). It is clear that the carcinoma cells displayed visible blue fluorescence, owing to the intense emission from TPE-OH NPs, suggesting that quantities of aggregated particles have been internalized into the cells (Figure 4). In contrast, no fluorescence could be

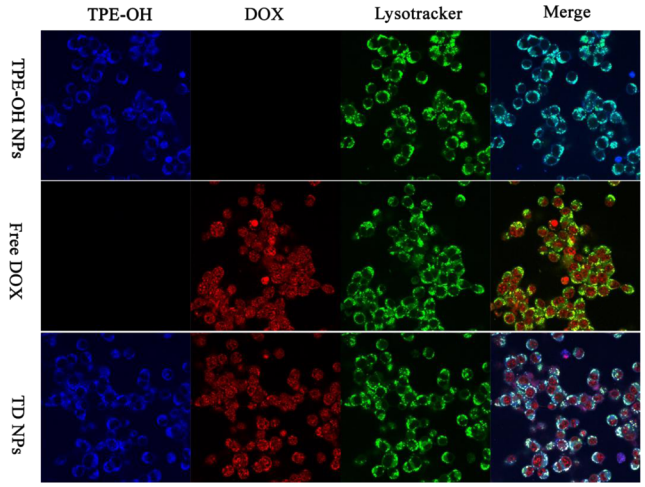

Figure 4. Confocal microscopy images of LL2 cells cultured with TPE-OH NPs (50 μM), free DOX (5 μM), TD NPs (50 μM), and costained with Lysotracker Green after a 4-h incubation.

detected in the control sample. The intracellular and intranuclear distributions of free DOX in LL2 cells were also observed through confocal laser scanning microscopy images (Figure 4). After incubation with TD NPs for 4 h, strong blue luminescence throughout the cell cytoplasm demonstrated that the substantial cellular uptakes of the regular nanospheres were possible. Simultaneously, remarkable increases of bright red emissions were found in the nucleoplasm of the cells treated with TD NPs relative to those treated with TPE-OH NPs (Figure 4). The cellular and nuclear uptakes of the new drug delivery system have been realized in a consecutive cell membrane-to-nuclear targeting manner. In this way, the anticancer drug was released from the nanocarrier due to the intracellular mild acidic conditions and translocated into the cell nucleus. The utilization of Lysotracker Green for the staining of lysosomes firmly proved that the location of TPE-

DOI: 10.1021/acs.jmedchem.5b01622
J. Med. Chem. XXXX, XXX, XXX−XXX

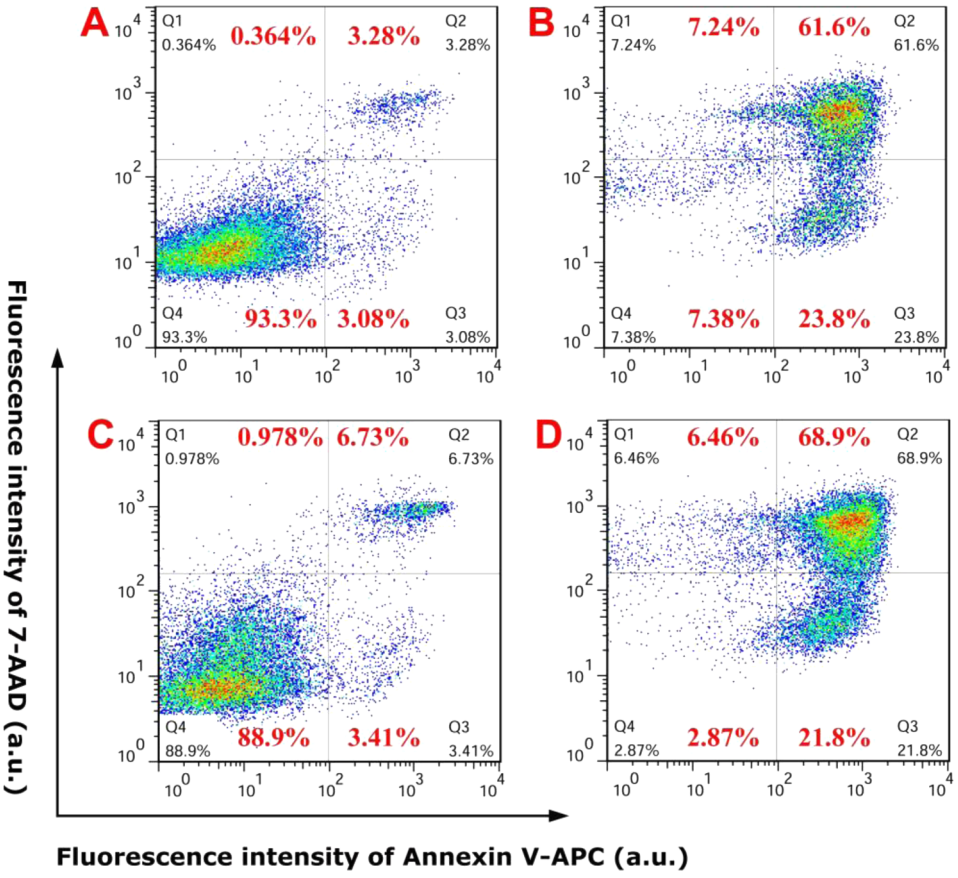

Figure 5. Representative distributions of THP-1 cells costained with Annexin V-APC/7-AAD. Cells were treated with (A) 0.5 μM DOX, (B) 5 μM DOX, (C) 5 μM TD NPs (0.5 μM DOX), or (D) 50 μM TD NPs (5 μM DOX) for 24 h prior to analysis. Viable cells are negative for both APC and 7-AAD (Q4 region), early apoptotic cells are APC positive and 7-AAD negative (Q3 region), late apoptotic or dead cells are positive, both APC and 7-AAD (Q2 region), while the damaged cells are APC negative and 7-AAD positive (located in the region of Q1).

OH NPs was nearly overlapped with lysosomes (Figure 4) and DOX could be efficiently delivered into nuclei of cancer cells (Figure 4). The intracellular controlled drug delivery process lies in the fact that the guest molecules would release depending on the interactions between TPE-OH NPs with negative surface charge and cationic DOX. It has been well accepted that dysregulated pH is a common indication of cancers, and lower pH environments in tumor cells were detected. New physiological pH sensitive vehicles hold promise for the therapeutic purpose of realizing high specificity. Here the decrease of pH would result in the dissociation of TD NPs, and the molecular electrostatic interactions were broken. Therefore, the released DOX from the AIE type carrier was internalized by tumor cells at lower pH, and improved cancer therapy efficiency could be achieved. To further explore the potential of using TD NPs as a simultaneous drug carrier and imaging sensor, two typical adherent cell lines (human breast adenocarcinoma, MCF-7, and human cervical cancer cells, HeLa) were incubated with TPE-OH NPs, free DOX and TD NPs, respectively (Figures S15 and 16). It can be seen that intense blue fluorescence signals are collected from the cytoplasm of cells and red emissions are highly accumulated in the nuclei in terms of the cell membrane to nuclear sequential strategy. In a subsequent study, the in vitro imaging behavior of a suspension cell line (human leukemic monocytic cells, THP-1) has been investigated (Figure S17). The results clearly demonstrated that TD NPs could not only be applied for targeted drug delivery, but also provide the possibility for real-time monitoring of luminescence changes in situ. Actually, to our knowledge, here is the first example of drug release visualization through tunable aggregation induced emission based on living suspension cells.

In vitro cytotoxicity analysis. The cytotoxicity of TPE-OH, free DOX, and TD NPs has been studied in the above-mentioned four cells by MTS assay, as given in Figures S18. After 24 h of incubation with TPE-OH, cell viabilities were all well above 90% of their original values, suggesting that TPE-OH particles have excellent biocompatibility in live cells. In general, the structural stability of TPE-OH might avoid disruption of live cells. Moreover, the presence of multiple aromatic moieties in TPE-OH may contribute to reduce the undesired toxicity due to the hydrophobic interactions with cell membranes. Additionally, the tightly packed structures would bind to lipid membranes with affinity and transmigrate into cells. However, when these cancer cells were treated with free DOX and TD NPs, a clear tendency of reduced cell viability was observed after 24 h. At each DOX dose concentration, the viability of cells incubated with TD NPs was slightly lower than that of free DOX molecules. This would be attributed to the improved DOX delivery efficiency within cancer cells by AIE edifices.

The DOX-triggered apoptosis process based on different drug-carrier forms has been explored by the flow cytometry. THP-1 cells were incubated with free DOX and TD NPs at various concentrations (Figure 5). Loading of pure DOX and TD NPs has led to a dramatic increase in the early and later

DOI: 10.1021/acs.jmedchem.5b01622
J. Med. Chem. XXXX, XXX, XXX−XXX

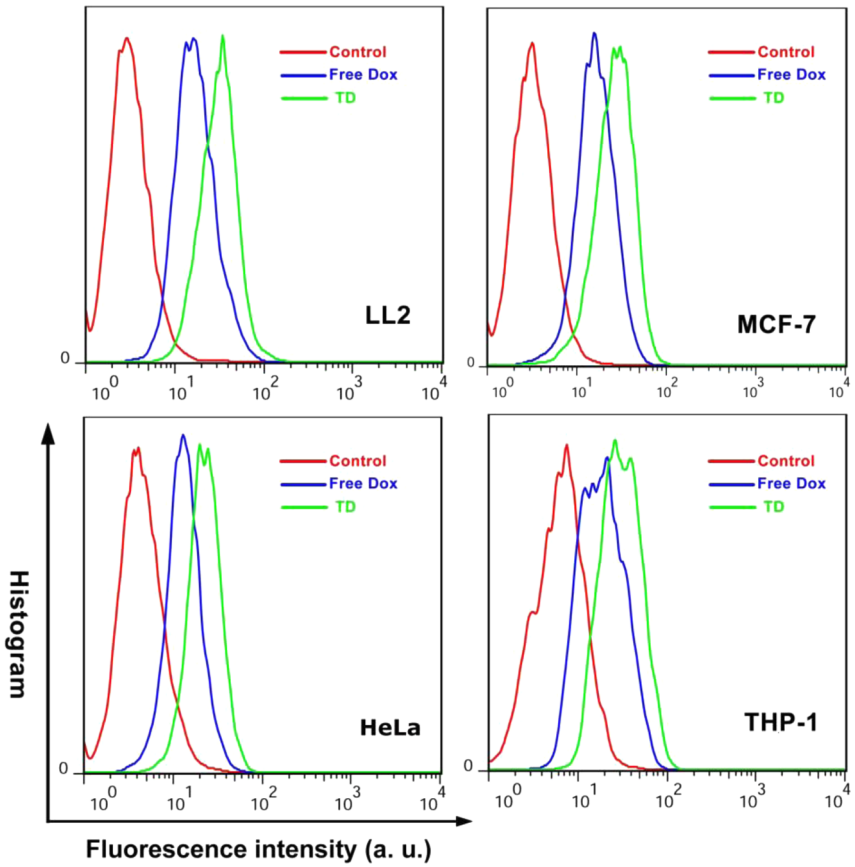

Figure 6. Fluorescence detected by flow cytometry in cells cultured with free DOX (1 μM) and TD NPs (10 μM) for 4 h.

apoptosis rates of the cells. In particular, the later apoptosis percentage reached 68.9%, which was higher than its counterpart (free DOX) and the result was in agreement with the previous experiments of the tumor cell viability. This enhanced therapeutic outcome demonstrated that the current AIE based delivery system was more efficient than individual DOX molecules. We further used flow cytometry to investigate the intracellular DOX concentrations. The collected curves confirmed that, although the concentrations of DOX and TD NPs in the culture medium remained the same, more DOX could be detected in the aforementioned four cancer cells incubated with TD NPs in contrast to the cells treated with pure DOX (Figure 6). The results showed that the transport of drug molecules across the cell membrane was more efficient when the drug was encapsulated in the nanocarrier.

Cellular entry mechanism. The rational design of luminescent sensors that can pass through cell membranes and enter a specific organelle needs a full understanding of the entry mechanism. Recent work has revealed that the nanoparticles are internalized into cells through two major uptake channels: passive diffusion and endocytosis. The latter energy-dependent case would be hindered at low temperature or under ATP-depleted conditions. As given in Figure S19–23, the studies performed at 4 °C or after ATP depletion presented very weak emissions in contrast to the normal conditions, indicating that the endocytosis pathway is the preferred process in the cellular internationalization. Since endocytosis takes many forms, the encapsulation of different inhibitors can disclose molecular components required for defining modes of cellular entry. The first chemical inhibitor (chlorpromazine) is a cationic amphipathic drug that induces the aggregation of adaptor proteins and clathrin and leads to depletion, thus blocking clathrin-mediated endocytosis. The results showed it causes an inhibition rate of around 60.6% on HeLa cells, suggesting that clathrin-mediated endocytosis was involved in the possible uptake ways. The second compound that could consistently inhibit macropinocytosis is cytochalasin D, which depolymerizes F-actin to suppress the process. An inhibition rate of 44.3% was achieved, demonstrating that this particular class of endocytosis (macropinocytosis) could be easily identified. Finally, we also included methyl-β-cyclodextran, which removes cholesterol from the plasma membrane and inhibits lipid raft mediated endocytotic pathways. The treatment of HeLa cells with methyl-β-cyclodextran did inhibit cellular uptake by approximately 49.2%. In addition, the systematic studies based on a number of inhibitors in three other cell lines showed slightly different yet generally similar results for the inhibition tests (Figures S20–S23). Consequently, it is estimated that clathrin-mediated endocytosis, macropinocytosis, and lipid raft-mediated endocytosis were all involved in the internalization mechanism. The selection from a screen of inhibitors for a targeted biochemical activity based on an aggregated-induced-emission (AIE) optical probe will contribute to a deeper understanding of the physiological functions.

In vivo anticancer efficiency. To determine whether TD NPs were effective within tumor-affected tissues, a tumor implantation mouse model was tested to assess the targeting capability. The experiments were performed by using a C57BL/6 mice model created subcutaneous inoculation with LL2 cancer cells. Then the extent of tumor growth was monitored.

DOI: 10.1021/acs.jmedchem.5b01622
J. Med. Chem. XXXX, XXX, XXX−XXX

In the parallel experiments, a single dose (at day 7) or two doses (at day 7 and day 14) of free DOX (5 mg/kg) and TD NPs (5 mg/kg) were intravenously injected into mice and administered on 18 days in each group. In the mice treated with 5 mg/kg of free DOX, a slight reduction in tumor volume was observed (Figure 7). However, the inhibitory effects derived

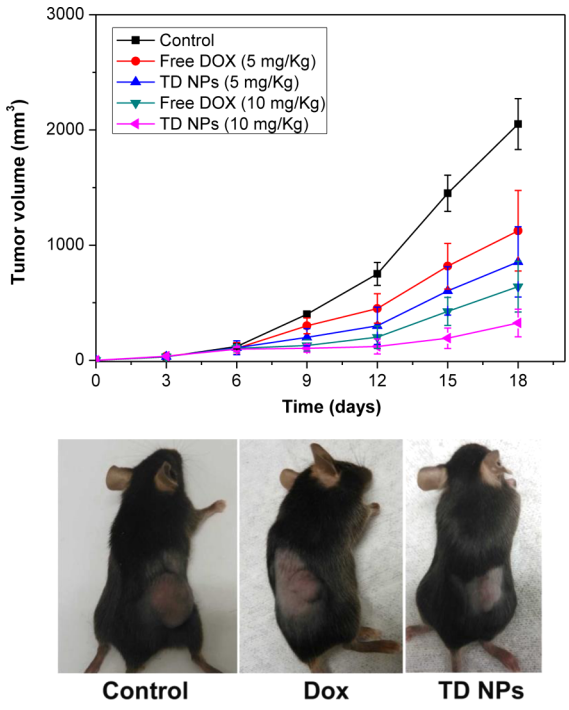

Figure 7. Quantitative analysis of the effects of various treatments on tumor size (top), and photos of mice after various treatments (bottom).

from TD NPs were demonstrated on a significant reduction in tumor volume compared with control and free DOX. This confirmed that the AIE-loaded new prodrug really works in terms of design purpose in vivo as well as in vitro. Since the treatment of DOX would induce negative responses or the decrease of white blood cell inside the human body, the total toxicity of free DOX and TD NPs has been studied. Mice treated with 10 mg/kg of TD NPs achieved almost equal body weight to that of control on day 9. At the planned end point (day 18), the mouse that was administered TD NPs was slightly heavier than the one treated with free DOX (Figure S24). This observation leads us to say that this new drug delivery system has less signs of toxicity compared with free drug. Generally, mice treated with anticancer drugs would show a weight loss due to serious side-effects in chemotherapy. Here the encapsulation of the drugs (free DOX) in the AIE delivery system would reduce systemic toxicity because of slower release in body fluid. The sustainable release from the nanovehicle could prevent the overexposure of DOX drugs to the normal cells. In addition, the tolerance capability of mice and their status might be different during the administration of drugs. Therefore, a gradual weight gain was achieved in the presence of TD NPs. To provide further evidence for the nanotoxicity of in vivo therapy, major organs such as lung, heart, liver, kidney, and spleen from the mice were collected. As shown in Figure 8, hematoxylin and eosin (H&E) stained images exhibited that no discernible signal of organ damages were identified from the

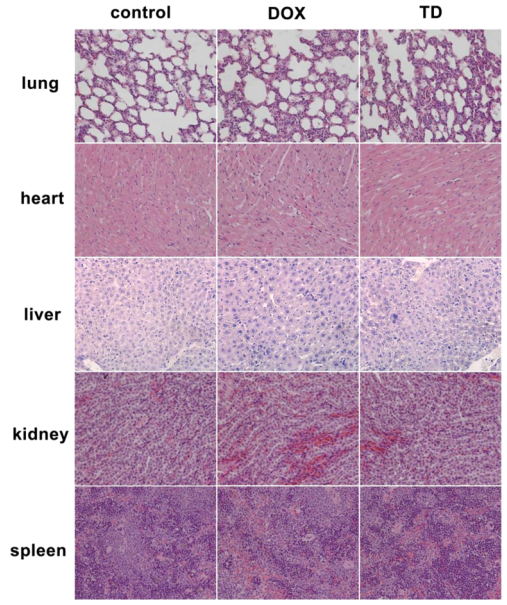

Figure 8. Representative H&E stained images of slices of indicated organs, including lung, heart, liver, kidney, and spleen, collected from mice treated with PBS, DOX (10 mg/kg), and TD (10 mg/kg) after 18 days.

organ slices, indicating that no appreciable toxic side effects have been found. Based on our results, doxorubicin formulated in TPE-OH nanoparticles induced apoptosis in cancer cell lines and had antitumor effects in vivo. It could effectively deliver DOX into tumor cells through visualization changes and show antiproliferative activity in animal models.

EXPERIMENTAL SECTION

Chemicals and materials. Benzophenone, 4-methoxybenzophenone, phosphorus tribromide, titanium(IV) chloride, doxorubicin hydrochloride (DOX), NaN_3, 2-deoxy-D-glucose, chlorpromazine, cytochalasin D, and methyl-β-cyclodextran were purchased from Sigma-Aldrich. Fetal bovine serum (FBS), antibiotics penicillin (PS), Dulbecco's modified medium (DMEM), and RPMI1640 medium were obtained from Life Technologies. The CellTiter 96 AQueous One Solution Reagent (MTS kit) was obtained from Promega. Lysotracker Green and the Annexin V-APC/7-AAD kit were purchased from BD Biosciences (USA). All the other chemicals were analytical reagents and used without further purification.

Synthesis of 1,1,2-triphenyl-2-(*p*-hydroxyphenyl)-ethene (compound 1). Zinc powder (1.56 g, 24 mmol) and anhydrous THF (40 mL) were added into a three-necked flask equipped with a magnetic stirrer under nitrogen atmosphere. The mixture was cooled to 0 to −5 °C, and 1.3 mL of $TiCl_4$ (12 mL) was slowly added. The suspension was warmed to room temperature. After 30 min, the mixture was heated with refluxing for 2.5 h. Then, the above solution was again cooled to 0 to −5 °C, charged with pyridine (0.5 mL, 6 mmol), and stirred for 10 min. The solution of a mixture of benzophenone (436 mg, 2.4 mmol) and 4-hydroxybezophenone (475 mg, 2.4 mmol) in 15 mL of THF was added slowly. Then, the reaction mixture was heated with refluxing for 10 h. Excess of 10% aqueous K_2CO_3 solution was added to quench the reaction, and product was taken up with CH_2Cl_2. The organic layer was collected, dried with anhydrous $NaSO_4$, and concentrated. The crude product was purified by column chromatography to obtain the target compound. ^{1}H NMR (400 MHz, DMSO-d_6): δ (ppm) 6.51 (d, J = 8.4 Hz, 2H), 6.74 (d, J = 8.4 Hz, 2H), 6.92−7.15 (m, 15H); Mass spectrum (ESI-MS): m/z 371.2 $[M + Na]^+$.

Preparation of TPE-OH NPs (nanoparticles of compound 1) and TD NPs. A solution of TPE-OH in DMSO was dropwise added

DOI: 10.1021/acs.jmedchem.5b01622
J. Med. Chem. XXXX, XXX, XXX−XXX

into water under vigorous stirring, and TPE-OH NPs were obtained after 5 min. Similarly, TD NPs were prepared first adding TPE-OH in DMSO dropwise into water and then adding DOX.

Photophysical studies. Fluorescence emission and excitation spectra were measured on a Hitachi F-2500. Absolute quantum yields were detected at room temperature through an integrating sphere (Hamamatsu C9920-02 system) method, and the sample was placed inside the integrating sphere. The excitation light was entered into the sphere by the optical fiber. When excitation wavelength (330 nm) was selected, the quantum yield values were calculated automatically by the software.

Cell lines and cell culture. Four cancer cell lines, LL2 (mouse lewis lung carcinoma cell), MCF-7 (human breast adenocarcinoma), HeLa (human cervical cancer cell), and THP-1 (human leukemic monocyte cell), were used in these studies. LL2, HeLa, and MCF-7 cells were cultured in Dulbecco's modified medium (DMEM) supplemented with 10% fetal bovine serum (FBS) and 1% antibiotics penicillin (PS) and maintained at 37 °C with 5% CO_2. THP-1 cells was incubated in RPMI 1640 medium supplemented with 10% fetal bovine serum (FBS) and 1% antibiotics penicillin (PS) and maintained at 37 °C with 5% CO_2.

MTS assay. The viability of LL2, HeLa, MCF-7, and THP-1 cells exposed to TPE-OH, free Dox, and TD was measured with MTS kits. The cells (about 5×10^3 cells/well) within replicate 96-well plates were precultured at standard culture conditions for 1 day. After removal of the medium, cells were incubated with fresh medium containing TPE-OH, free Dox, or TD (with various concentration) for another 24 h. Twenty μL MTS solution was added to each well. After incubation for 2 h, the absorbance at 490 nm using a Polarsar microplate reader was recorded.

Flow cytometry and apoptosis analysis. Flow cytometry and apoptosis assays were performed as we described.[37,38] Briefly, the above-mentioned four kinds of cells were cultured with free Dox (1 μM) and TD NPs (10 μM) for 2 h, respectively. Then, cells were washed and resuspended in PBS, and measured by flow cytometry on a BD Accuri C6 Flow Cytometer. To investigate apoptosis analysis, untreated cells and cells treated with Dox (0.5 or 5 μM) and TD NPs (5 or 50 μM) were both stained with Annexin V-APC/7-AAD. THP-1 cells (5×10^5 cells/well) were dispersed within replicated 12-well microtiter plates and incubated for 24 h at 37 °C with 5% CO_2. After removal of the medium, cells were incubated with fresh medium (here fresh medium refers to DMEM supplemented with 10% fetal bovine serum and 1% antibiotics penicillin or RPMI 1640 medium supplemented with 10% fetal bovine serum and 1% antibiotics penicillin) containing Dox (0.5 or 5 μM) and TD NPs (5 or 50 μM) for another 24 h. After washing with binding buffer twice, centrifuging, and adding another 100 μL binding buffer, 3 μL of 7-AAD and Annexin V-PE were added to each sample. Samples were incubated for 15 min and analyzed by flow cytometry.

Cell imaging. Cell imaging was performed as we described.[39] Briefly, the cells were plated in Lab-Tek chambered cover glass (8-well, Thermo Scientific, USA) with a density of 10^4 cells/mL and grown to 70% confluency. The cells were washed with medium and incubated in the fresh medium containing TPE-OH NPs (50 μM), DOX (5 μM), or TD NPs (50 μM) for another 4 h. Cells were washed three times with PBS and costained with Lysotracker Green (200 nM for 20 min), then imaged on a Leica confocal laser scanning microscope (TCS SP2 AOBS).

Intracellular transport mechanism. First, the energy-dependent uptake was performed with low temperature incubation and ATP depletion treatments. The four cell lines (LL2, HeLa, MCF-7, and THP-1) cultured at standard culture conditions were treated with TD NPs (50 μM) and immediately maintained at 4 °C for 2 h. For the ATP-depleted environments, cells were preincubated with 2-deoxy-D-glucose (50 mM) and sodium azide (10 mM) for 30 min at 37 °C; subsequently, cells were washed with PBS three times and then incubated with TD NPs (50 μM). The intracellular fluorescence intensity of TD NPs was detected using flow cytometry. Second, three different inhibitors (chlorpromazine, cytochalasin D, methyl-β-cyclodextran) were used to determine the modes of endocytosis. Cells (5×10^5 cells/well) were seeded in 12-well plates and incubated for 24 h. Chlorpromazine (10 μg/mL) and cytochalasin D (5 μM), or methyl-β-cyclodextran (5 mg/mL) were added into the medium and cultured at 37 °C for 45 min. TD NPs (50 μM) were then added and incubated for another 2 h. Then, cells were washed with PBS three times, centrifuged, and resuspended in PBS. The cellular uptake efficiency was determined using a flow cytometer.

In vivo studies. The LL2 implantation experiment was performed as we described.[40] Briefly, 1×10^6 cells in 200 μL PBS were injected subcutaneously into the female C57BL/6 mice (4–6 weeks old). When the tumors reached a size of approximately 100 mm^3 (at day 7), the mice were divided into several groups for subsequent experiments.

Mice bearing LL2 tumors in different groups were intravenous injected with free DOX (5 mg/kg, single dose at day 7), free DOX (10 mg/kg, two doses at day 7 and 14), and TD NPs (5 mg/kg, single dose at day 7), TD NPs (10 mg/kg, two doses at day 7 and 14), respectively. Tumor size was measured with a digital caliper every three days, and tumor volume was calculated by (length of tumor) × (width of tumor)^2/2. The body weight of mice without tumors was also monitored. After 18 days, the major organs of those mice were collected and fixed in 4% formalin for at least 3 days. The tissues were stained with hematoxylin and eosin (H&E), and observed under a BX50 bright field microscope (Olympus).

Measurements. ^{1}H NMR spectra were recorded at 293 K using a Varian 400 (400 MHz) with TMS as an internal standard; all chemical shifts were reported in the standard notation of parts per million. LC-MS was measured on a Thermo Finnigan LCQ Deca XP Max. FT-IR spectra were measured using a Shimadzu Prestige-21. TEM was measured using a JEOL JEM-2100HR transmission electron microscope. Energy dispersive X-ray (EDX) analysis data were measured based on a scanning electron microscope equipped with an energy-dispersive spectrometer (S-4800, Hitachi, Japan). The surface charges of TPE-OH and TD-NPs were measured through dynamic light scattering (Malvern Zetasizer Nano ZS90).

CONCLUSIONS

As our understanding of different drug delivery systems increases, it becomes more important to embrace one particular drug carrier as a new diagnostic tool for a specific mode of therapy. Here the use of aggregation induced emission type compounds appears to offer better choices than the conventional fluorophores. Based on our findings, TPE-OH NPs exhibited very weak fluorescence signals in organic solvents. But the exposure to aqueous solution induces a 60-fold increase in the emission intensity. The drug loaded nanoassembly (TD NPs) could be internalized effectively within four sorts of cancer cells (including three adherent cell lines and one suspension cell line). The excellent biocompatibility showed that this AIE based nanoprobe possessed the potential as a cell imaging agent and antitumor drug carrier simultaneously. The identification of energy-dependent uptake and the use of inhibitors will be valuable as we start to figure out the physiological functions and mechanisms of cellular entry derived from a new theranostic system. More importantly, it allows one to target the drug release and evaluate the therapeutic efficiency in vivo, which is fundamental in developing novel responsive materials in clinical cancer treatment.

ASSOCIATED CONTENT

Supporting Information

The Supporting Information is available free of charge on the ACS Publications website at DOI: 10.1021/acs.jmedchem.5b01622.

Synthesis of TPE-OH; photoluminescence spectra of TPE-OH NPs, TD NPs, and free DOX; overlap of the

DOI: 10.1021/acs.jmedchem.5b01622
J. Med. Chem. XXXX, XXX, XXX−XXX

absorption spectra of DOX and the emission spectra of TPE-OH; fuorescence spectra of TD NPs when dispersed in various pH buffers; TEM image of TPE-OH nanoparticles; fluorescence changes of TPE-OH when adding different molar ratios of DOX; confocal microscopy images of MCF-7, HeLa, and THP-1; cell viability of TPE-OH, free Dox, and TD NPs toward various cells; study on the mechanism of cell uptake; body weight changes of mice in the presence of different treatments. (PDF)

AUTHOR INFORMATION

Corresponding Author

*Tel.: 86-20-39310258. Fax: 86-20-39310187. E-mail address: qmwang@scnu.edu.cn.

Notes

The authors declare no competing financial interest.

ACKNOWLEDGMENTS

Q.W. acknowledges the support from the National Natural Science Foundation of China (grants number 21371063 and 21328503), an excellent university young scholar fund of Guangdong province (Yq2013053), the Guangzhou city scientific research fund (2014J4100054), the Guangdong Science and Technology plan (2013B010403025), and the Natural Science Foundation of Guangdong (2015A030313378). Support to C.C.Z. was from Leukemia & Lymphoma Society Award 1024-14 and CPRIT RP140402. Z.Z. acknowledges the China Scholarship Council (CSC) for financial support.

ABBREVIATIONS USED

AIE, aggregated-induced-emission; TPE-OH, 1,1,2-triphenyl-2-(*p*-hydroxyphenyl)-ethene; TPE-OH NPs, 1,1,2-triphenyl-2-(*p*-hydroxyphenyl)-ethene nanoparticles; DOX, doxorubicin hydrochloride; TD NPs, 1,1,2-triphenyl-2-(*p*-hydroxyphenyl)-ethene doxorubicin hydrochloride nanoparticles; LL2, mouse lewis lung carcinoma cell; HeLa, human cervical cancer cell; THP-1, human leukemic monocyte cell; MCF-7, human breast adenocarcinoma; H&E, hematoxylin and eosin; FBS, fetal bovine serum; PS, antibiotics penicillin; DMEM, Dulbecco's modified medium; ATP, adenosine triphosphate; APC, allophycocyanin; MTS, 3-(4,5-dimethylthiazol-2-yl)-5-(3-carboxymethoxyphenyl)-2-(4-sulfophenyl)-2H-tetrazolium; 7-AAD, 7-aminoactinomycin D; TEM, transmission electron microscope; NMR, nuclear magnetic resonance

REFERENCES

(1) Bouzin, C.; Feron, O. Targeting tumor stroma and exploiting mature tumor vasculature to improve anti-cancer drug delivery. *Drug Resist. Updates* **2007**, *10*, 109−120.

(2) Jain, R. K. Delivery of molecular and cellular medicine to solid tumors. *Adv. Drug Delivery Rev.* **2001**, *46*, 149−168.

(3) Kouranos, V.; Dimopoulos, G.; Vassias, A.; Syrigos, K. N. Chemotherapy-induced neutropenia in lung cancer patients: the role of antibiotic prophylaxis. *Cancer Lett.* **2011**, *313*, 9−14.

(4) Trachootham, D.; Alexandre, J.; Huang, P. Targeting cancer cells by ROS-mediated mechanisms: a radical therapeutic approach? *Nat. Rev. Drug Discovery* **2009**, *8*, 579−591.

(5) Peer, D.; Karp, J. M.; Hong, S.; Farokhzad, O. C.; Margalit, R.; Langer, R. Nanocarriers as an emerging platform for cancer therapy. *Nat. Nanotechnol.* **2007**, *2*, 751−760.

(6) Yin, W. Y.; Yan, L.; Yu, J.; Tian, G.; Zhou, L. J.; Zheng, X. P.; Zhang, X.; Yong, Y.; Li, J.; Gu, Z. J.; Zhao, Y. L. High-throughput synthesis of single-layer MoS_2 nanosheets as a near-infrared photothermal-triggered drug delivery for effective cancer therapy. *ACS Nano* **2014**, *8*, 6922−6933.

(7) Li, L. L.; Tang, F. Q.; Liu, H. Y.; Liu, T. L.; Hao, N. J.; Chen, D.; Teng, X.; He, J. Q. In vivo delivery of silica nanorattle encapsulated docetaxel for liver cancer therapy with low toxicity and high efficacy. *ACS Nano* **2010**, *4*, 6874−6882.

(8) Chen, Y.; Tan, C. L.; Zhang, H.; Wang, L. Z. Two-dimensional graphene analogues for biomedical applications. *Chem. Soc. Rev.* **2015**, *44*, 2681−2701.

(9) Wang, K.; Zhang, X. H.; Zhang, X. Q.; Yang, B.; Li, Z.; Zhang, Q. S.; Huang, Z. F.; Wei, Y. Fabrication of cross-linked fluorescent polymer nanoparticles and their cell imaging applications. *J. Mater. Chem. C* **2015**, *3*, 1854−1860.

(10) Qin, W.; Ding, D.; Liu, J. Z.; Yuan, W. Z.; Hu, Y.; Liu, B.; Tang, B. Z. Biocompatible nanoparticles with aggregation-induced emission characteristics as far-red/near-infrared fluorescent bioprobes for in vitro and in vivo imaging applications. *Adv. Funct. Mater.* **2012**, *22*, 771−779.

(11) Zhu, H. B.; Li, Y. X.; Qiu, R. Q.; Shi, L.; Wu, W. T.; Zhou, S. Q. Responsive fluorescent Bi_2O_3@PVA hybrid nanogels for temperature-sensing, dual-modal imaging, and drug delivery. *Biomaterials* **2012**, *33*, 3058−3069.

(12) Shi, J. J.; Yu, X. Y.; Wang, L.; Liu, Y.; Gao, J.; Zhang, J.; Ma, R.; Liu, R. Y.; Zhang, Z. Z. PEGylated fullerene/iron oxide nanocomposites for photodynamic therapy, targeted drug delivery and MR imaging. *Biomaterials* **2013**, *34*, 9666−9677.

(13) Ge, J.; Neofytou, E.; Cahill, T. J., III; Beygui, R. E.; Zare, R. N. Drug release from electric-field-responsive nanoparticles. *ACS Nano* **2012**, *6*, 227−233.

(14) Lovell, J. F.; Jin, C. S.; Huynh, E.; MacDonald, T. D.; Cao, W. G.; Zheng, G. Enzymatic regioselection for the synthesis and biodegradation of porphysome nanovesicles. *Angew. Chem.* **2012**, *124*, 2479−2483.

(15) Marin, A.; Muniruzzaman, M.; Rapoport, N. Acoustic activation of drug delivery from polymeric micelles: effect of pulsed ultrasound. *J. Controlled Release* **2001**, *71*, 239−249.

(16) Bhuniya, S.; Maiti, S.; Kim, E. J.; Lee, H.; Sessler, J. L.; Hong, K. S.; Kim, J. S. An activatable theranostic for targeted cancer therapy and imaging. *Angew. Chem.* **2014**, *126*, 4558−4563.

(17) Krall, N.; Pretto, F.; Decurtins, W.; Bernardes, G. J. L.; Supuran, C. T.; Neri, D. A small-molecule drug conjugate for the treatment of carbonic anhydrase IX expressing tumors. *Angew. Chem., Int. Ed.* **2014**, *53*, 4231−4235.

(18) Zhao, Z.; Chen, S. M.; Shen, X. Y.; Mahtab, F.; Yu, Y.; Lu, P.; Lam, J. W. Y.; Kwok, H. S.; Tang, B. Z. Aggregation-induced emission, self-assembly, and electroluminescence of 4,4′-bis (1, 2, 2-triphenylvinyl) biphenyl. *Chem. Commun.* **2010**, *46*, 686−688.

(19) Hong, Y. N.; Lam, J. W. Y.; Tang, B. Z. Aggregation-induced emission. *Chem. Soc. Rev.* **2011**, *40*, 5361−5388.

(20) Wu, J. S.; Liu, W. M.; Ge, J. G.; Zhang, H. Y.; Wang, P. F. New sensing mechanisms for design of fluorescent chemosensors emerging in recent years. *Chem. Soc. Rev.* **2011**, *40*, 3483−3495.

(21) Shimizu, M.; Takeda, Y.; Higashi, M.; Hiyama, T. 1,4-Bis (alkenyl)-2, 5-dipiperidinobenzenes: minimal fluorophores exhibiting highly efficient emission in the solid state. *Angew. Chem.* **2009**, *121*, 3707−3710.

(22) Shustova, N. B.; McCarthy, B. D.; Dinca, M. Turn-on fluorescence in tetraphenylethylene-based metal-organic frameworks: an alternative to aggregation-induced emission. *J. Am. Chem. Soc.* **2011**, *133*, 20126−20129.

(23) Yuan, Y.; Kwok, R. T.; Tang, B. Z.; Liu, B. Targeted theranostic platinum (IV) prodrug with a built-in aggregation-induced emission light-up apoptosis sensor for noninvasive early evaluation of its therapeutic responses in situ. *J. Am. Chem. Soc.* **2014**, *136*, 2546−2554.

DOI: 10.1021/acs.jmedchem.5b01622
J. Med. Chem. XXXX, XXX, XXX−XXX

(24) Peng, L. H.; Wang, M.; Zhang, G. X.; Zhang, D. Q.; Zhu, D. B. A fluorescence turn-on detection of cyanide in aqueous solution based on the aggregation-induced emission. *Org. Lett.* **2009**, *11*, 1943−1946.
(25) Duan, X. F.; Zeng, J.; Lü, J. W.; Zhang, Z. B. Insights into the general and efficient cross McMurry reactions between ketones. *J. Org. Chem.* **2006**, *71*, 9873−9876.
(26) Liu, Y.; Chen, S. M.; Lam, J. W. Y.; Lu, P.; Kwok, R. T. K.; Mahtab, F.; Kwok, H. S.; Tang, B. Z. Tuning the electronic nature of aggregation-induced emission luminogens with enhanced hole-transporting property. *Chem. Mater.* **2011**, *23*, 2536−2544.
(27) Tang, J.; Kong, B.; Wu, H.; Xu, M.; Wang, Y. C.; Wang, Y. L.; Zhao, D. Y.; Zheng, G. F. Carbon nanodots featuring efficient FRET for real-time monitoring of drug delivery and two-photon imaging. *Adv. Mater.* **2013**, *25*, 6569−6574.
(28) Bagalkot, V.; Zhang, L. F.; Levy-Nissenbaum, E.; Jon, S.; Kantoff, P. W.; Langer, R.; Farokhzad, O. C. Quantum dot-aptamer conjugates for synchronous cancer imaging, therapy, and sensing of drug delivery based on bi-fluorescence resonance energy transfer. *Nano Lett.* **2007**, *7*, 3065−3070.
(29) Chen, W. S.; Huang, Q. Y.; Ou, W. Z.; Hao, Y. Q.; Wang, L. Q.; Zeng, K.; Guo, H. Y.; Li, J.; Liu, Y. N. Self-reporting liposomes for intracellular drug release. *Small* **2014**, *10*, 1261−1265.
(30) Gillies, E. R.; Fréchet, J. M. pH-responsive copolymer assemblies for controlled release of doxorubicin. *Bioconjugate Chem.* **2005**, *16*, 361−368.
(31) Tang, N.; Du, G. F.; Wang, N.; Liu, C. C.; Hang, H. Y.; Liang, W. Improving penetration in tumors with nanoassemblies of phospholipids and doxorubicin. *J. Natl. Cancer Inst.* **2007**, *99*, 1004−1015.
(32) Wang, T. T.; Bai, J.; Jiang, X.; Nienhaus, G. U. Cellular uptake of nanoparticles by membrane penetration: a study combining confocal microscopy with FTIR spectroelectrochemistry. *ACS Nano* **2012**, *6*, 1251−1259.
(33) Farokhzad, O. C.; Langer, R. Impact of nanotechnology on drug delivery. *ACS Nano* **2009**, *3*, 16−20.
(34) Xue, X. D.; Zhao, Y. Y.; Dai, L. R.; Zhang, X.; Hao, X. D.; Zhang, C. Q.; Huo, S. D.; Liu, J.; Liu, C.; Kumar, A.; Chen, W. Q.; Zou, G. Z. Spatiotemporal drug release visualized through a drug delivery system with tunable aggregation-induced emission. *Adv. Mater.* **2014**, *26*, 712−717.
(35) Qin, W.; Ding, D.; Liu, J. Z.; Yuan, W. Z.; Hu, Y.; Liu, B.; Tang, B. Z. Biocompatible nanoparticles with aggregation-Induced emission characteristics as far-red/near-infrared fluorescent bioprobes for in vitro and in vivo imaging applications. *Adv. Funct. Mater.* **2012**, *22*, 771−779.
(36) Zhang, X. Q.; Zhang, X. Y.; Wang, S. Q.; Liu, M. Y.; Tao, L.; Wei, Y. Surfactant modification of aggregation-induced emission material as biocompatible nanoparticles: facile preparation and cell imaging. *Nanoscale* **2013**, *5*, 147−150.
(37) Zheng, J. K.; Umikawa, M.; Cui, C. H.; Li, J. Y.; Chen, X. L.; Zhang, C. Z.; Huynh, H.; Kang, X. L.; Silvany, R.; Wan, X.; Ye, J. X.; Cantó, A. P.; Chen, S. H.; Wang, H. Y.; Ward, E. S.; Zhang, C. C. Inhibitory receptors bind ANGPTLs and support blood stem cells and leukaemia development. *Nature* **2012**, *485*, 656−660.
(38) Kang, X. L.; Lu, Z. G.; Cui, C. H.; Deng, M.; Fan, Y. Q.; Dong, B. J.; Han, X.; Xie, F. C.; Tyner, J. W.; Coligan, J. E.; Collins, R. H.; Xiao, X. S.; You, M. J.; Zhang, C. C. The ITIM-containing receptor LAIR1 is essential for acute myeloid leukaemia development. *Nat. Cell Biol.* **2015**, *17*, 665−677.
(39) Zheng, J. K.; Huynh, H.; Umikawa, M.; Silvany, R.; Zhang, C. C. Angiopoietin-like protein 3 supports the activity of hematopoietic stem cells in the bone marrow niche. *Blood* **2011**, *117*, 470−479.
(40) Huynh, H.; Zheng, J. K.; Umikawa, M.; Silvany, R.; Xie, X. J.; Wu, C. J.; Holzenberger, M.; Wang, Q.; Zhang, C. C. Components of the hematopoietic compartments in tumor stroma and tumor-bearing mice. *PLoS One* **2011**, *6*, e18054.

DOI: 10.1021/acs.jmedchem.5b01622
J. Med. Chem. XXXX, XXX, XXX−XXX